Final publication is available from Mary Ann Liebert, Inc., publishers:
Garske, D., Schmidt-Bleek, K., Ellinghaus, A., Dienelt, A., Gu, L., Mooney, D. J., et al. (2020). Alginate hydrogels for in vivo bone regeneration: the immune competence of the animal model matters. Tissue Engineering Part A, 26(15-16), 852-862. doi:10.1089/ten.TEA.2019.0310.

Alginate hydrogels for *in vivo* bone regeneration: the immune competence of the animal model matters

D. S. Garske, K. Schmidt-Bleek, A. Ellinghaus, A. Dienelt,
L. Gu, D. J. Mooney, G. N. Duda, A. Cipitria

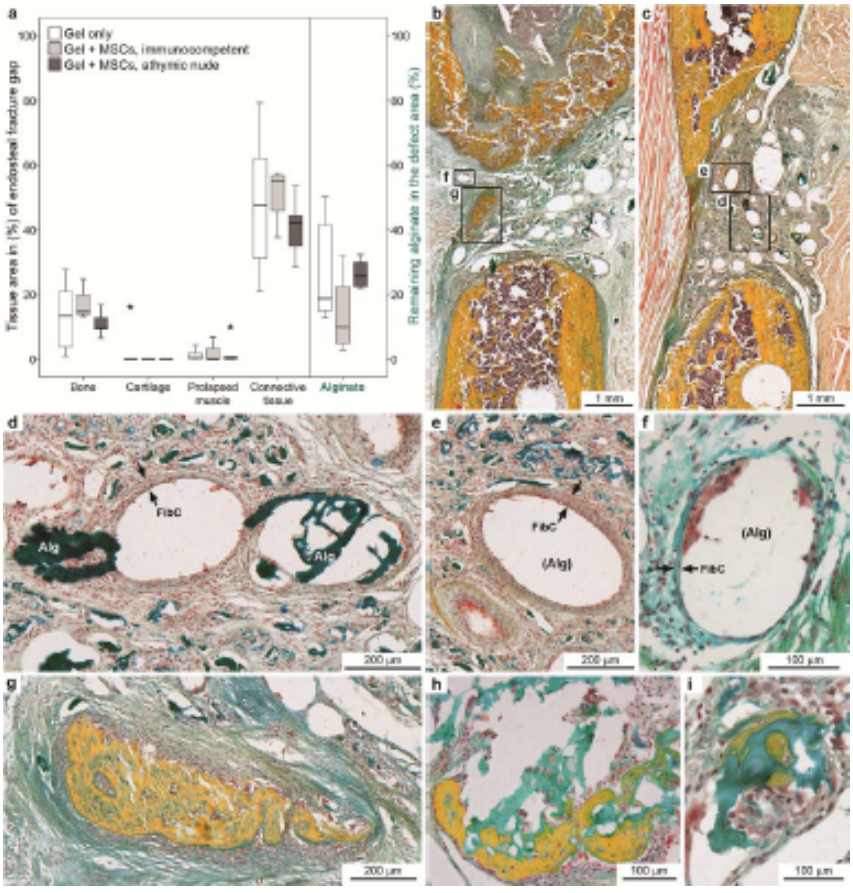

Alginate Hydrogels for *In Vivo* Bone Regeneration: The Immune Competence of the Animal Model Matters

Daniela S. Garske, M.Sc.[1,2], Katharina Schmidt-Bleek, Ph.D.[1], Agnes Ellinghaus, Dr.med.vet.[1], Anke Dienelt, Ph.D.[1,3], Luo Gu, Prof.[4,5,6], David J. Mooney, Prof.[4,5], Georg N. Duda, Prof.[1,3], *Amaia Cipitria, Ph.D.[1,2,3]

[1] Julius Wolff Institute & Center for Musculoskeletal Surgery, Charité - Universitätsmedizin Berlin, 13353 Berlin, Germany

[2] Max Planck Institute of Colloids and Interfaces, Department of Biomaterials, 14476 Potsdam, Germany

[3] Berlin-Brandenburg Center for Regenerative Therapies, Charité - Universitätsmedizin Berlin, 13353 Berlin, Germany

[4] School of Engineering and Applied Sciences, Harvard University, Cambridge, MA 02138, USA

[5] Wyss Institute for Biologically Inspired Engineering, Harvard University, Boston, MA 02115, USA

[6] Department of Materials Science and Engineering, Institute for Nanobiotechnology, Johns Hopkins University, Baltimore, MD, 21218, USA

* Corresponding author

Amaia Cipitria, Ph.D.

Tel: +49 (0)331 567-9452

Email: amaia.cipitria@mpikg.mpg.de

List of authors

- Daniela S. Garske, M.Sc.
  Tel: +49 (0)331 567-9461
  Email: Daniela.Garske@mpikg.mpg.de
- Katharina Schmidt-Bleek, Ph.D.
  Tel: +49 (0)30 450 659209
  Email: Katharina.Schmidt-Bleek@charite.de
- Agnes Ellinghaus. Dr.med.vet.
  Tel: +49 (0)30 450 659027
  Email: Agnes.Ellinghaus@charite.de
- Anke Dienelt, Ph.D.
  Tel: +49 (0)174 9356940
  Email: Anke.Dienelt@gmx.de
- Luo Gu, Prof.
  Tel: +1 (410) 516-8765
  Email: luogu@jhu.edu
- David J. Mooney, Prof.
  Tel: +1 (617) 384-9624
  Email: mooneyd@seas.harvard.edu
- Georg N. Duda, Prof.
  Tel: +49 (0)30 450 659079
  Email: Georg.Duda@charite.de

Keywords: alginate, hydrogel, bone regeneration, critical-sized bone defect, immune system, animal model

Abstract

Biomaterials with tunable biophysical properties hold great potential for tissue engineering. The adaptive immune system plays an important role in bone regeneration. Our goal is to investigate the regeneration potential of cell-laden alginate hydrogels depending on the immune status of the animal model. Specifically, the regeneration potential of rat mesenchymal stromal cell (MSC)-laden, void-forming alginate hydrogels, with a stiffness optimized for osteogenic differentiation, is studied in 5 mm critical-sized femoral defects, in both T-cell deficient athymic RNU nude rats and immunocompetent Sprague Dawley rats. Bone volume fraction, bone mineral density and tissue mineral density are higher for athymic RNU nude rats 6 weeks post-surgery. Additionally, these animals show a significantly higher number of total cells and cells with non-lymphocyte morphology at the defect site, while the number of cells with lymphocyte-like morphology is lower. Hydrogel degradation is slower and the remaining alginate fragments are surrounded by a thicker fibrous capsule. Ossification islands originating from alginate residues suggest that encapsulated MSCs differentiate into the osteogenic lineage and initiate the mineralization process. However, this effect is insufficient to fully bridge the bone defect in both animal models. Alginate hydrogels can be used to deliver MSCs and thereby recruit endogenous cells through paracrine signaling, but additional osteogenic stimuli are needed to regenerate critical-sized segmental femoral defects.

Impact Statement

T-cell deficient athymic RNU nude rats are commonly used to evaluate the regeneration potential of biomaterials in combination with cells of human origin. In this study we show that the effect of MSC-laden alginate hydrogels on bone regeneration differs depending of the immune status of the animal model. Furthermore, while alginate hydrogels are interesting materials to investigate the effect tunable biophysical properties on cell response and *in vivo* regeneration, their use in combination with rat MSCs is insufficient to fully bridge critical-sized segmental femoral defects. For this purpose, additional osteogenic stimuli such as growth factor delivery are necessary.

Introduction

The regeneration of load-bearing, critical-sized bone defects remains an unmet clinical need.[1] Biomaterials with tunable biophysical properties hold great potential for bone tissue engineering[2]. Pioneering work by Pelham and Wang [3] and Engler and colleagues [4] showed that cells sense and respond to substrate stiffness. Those fundamental studies with mesenchymal stromal cells (MSCs) on two dimensional (2D) hydrogel substrates were then extended to 3D matrices.[5] MSCs encapsulated in ionically crosslinked alginate hydrogels differentiated towards osteogenic or adipogenic lineages in stiff (11-30 kPa) or soft (2.5-5 kPa) gels, respectively. More recently, matrix viscoelasticity has emerged as another important tissue property that cells respond to.[6] Mouse MSC spreading, proliferation and osteogenic differentiation were enhanced in fast relaxing viscoelastic alginate gels, compared to elastic hydrogels, for a stiffness range optimized for osteogenic differentiation.

Elasticity and viscoelasticity-mediated *in vitro* osteogenesis were evaluated *in vivo* by Mooney and colleagues, in a non-load bearing, 8 mm critical-sized cranial defect model in T-cell deficient athymic RNU nude rats.[7, 8] For the former, composite biomaterials were used to decouple stiffness from degradability, with (i) human MSCs encapsulated in an ionically-crosslinked alginate bulk phase with a stiffness optimized for osteogenic differentiation, and (ii) degradable alginate porogens mixed in the bulk phase to allow for cell proliferation, migration and tissue formation. A stiffness-dependent increase in bone volume was observed after 3 months.[7] For the latter, hydrogels with the same stiffness but different stress relaxation rates, and with encapsulated human MSCs, were implanted and significantly higher bone volume was measured in faster relaxing gels after 3 months.[8] Still, none of these materials were successful in fully bridging the critical-sized cranial defect.

Recently, cell-free, void-forming alginate hydrogels, analogous to the injectable gels used by Huebsch and colleagues,[7] were evaluated for their bone regeneration potential in a load-bearing, 5 mm critical-sized segmental femoral defect in immunocompetent Sprague Dawley rats.[9] The in-situ bone regeneration strategy relied on the (i) delivery of stromal cell-derived factor-1α (SDF-1α) for the recruitment of host bone marrow-derived stromal

cells (BMSC) to the defect site and (ii) stiffness-mediated osteogenic differentiation of invading BMSC into the void-forming hydrogels. Increased bone volume fraction and bone mineral density was observed after 2 weeks, yet this effect vanished with time and was not sufficient to bridge the bone defect after 6 weeks.

The regeneration mechanisms in cell-laden vs. acellular hydrogels are clearly different. It has been shown that the response of MSCs to substrate stiffness differs if the cells are encapsulated in the gel or spread within the pores of a 3D scaffold, due to the broad range of possible cell orientations within the pores, which translates into different mechanical stimuli.[10] Furthermore, in addition to the ability to differentiate into different lineages, MSCs can also support tissue regeneration through paracrine signaling by secretion of bioactive molecules.[11-15]

Furthermore, the immune competence of the animal model also plays a role in *in vivo* bone regeneration. The adaptive immune system regulated by lymphocytes orchestrates to a large extent the bone healing process.[16-18] Tibia fracture healing was investigated in γ/δ T-cell deficient mice and superior biomechanical strength, more mature histologic features and decreased IL-6 pro-inflammatory cytokines were observed compared to wild-type controls.[19] Femoral fracture healing was investigated in knockout $RAG1^{-/-}$ mice lacking the adaptive immune system and accelerated mineralization, decreased pro-inflammatory cytokines and upregulation of IL-10 anti-inflammatory cytokines were measured.[20] In a follow-up study, it was shown that accumulation of $CD8^+$ $T_{cytotoxic}$ lymphocytes impaired bone regeneration in a mouse osteotomy model, while depletion of $CD8^+$ $T_{cytotoxic}$ lymphocytes improved the regeneration outcome.[21] This was in agreement with increased levels of $CD8^+$ $T_{cytotoxic}$ lymphocytes in the peripheral blood of human patients, which was associated with delayed bone regeneration.[21] Last, changes in the collagen organization process, osteoblast distribution and stiffness of the newly formed bone have been reported in a bone fracture model in mice lacking mature T cells.[22] This raises the question whether *in vivo* bone regeneration is enhanced in T-cell deficient athymic RNU nude rats.

The main goal of this study is to investigate the regeneration potential of cell-laden alginate hydrogels as a function of the immune status of the animal model. MSC-laden, void-forming alginate hydrogels are investigated in load-bearing, 5 mm critical-sized segmental femoral defects, in both T-cell deficient athymic RNU nude rats and immunocompetent Sprague Dawley rats (**Figure 1**). The composite hydrogels consist of (i) an ionically-crosslinked alginate bulk phase with a stiffness optimized for osteogenic differentiation, (ii) rat MSCs encapsulated in the bulk gel optimized for osteogenesis and (iii) degradable alginate porogens mixed in the bulk phase to allow for cell migration, proliferation and tissue formation.

Materials and Methods

MSC-laden void-forming alginate hydrogels

The fabrication of void-forming hydrogels has been described previously.[7, 9] Briefly, ultrapure, high molecular weight (265 kg/mol), high guluronic acid (HMW-MVG unmodified) sodium alginate (FMC BioPolymer, Novamatrix) was used as base polymer. The linear cell adhesion peptide G_4RGDSP (Peptide 2.0) was introduced by carbodiimide chemistry, with a degree of substitution of 10 peptides per alginate chain.

The synthesis of hydrolytically degradable alginate porogens has been described previously.[7, 9] The lyophilized, alginate porogens were rehydrated in serum-free DMEM, with low glucose, no glutamine, no phenol red and pH adjusted to 7.4 $\pm$ 0.15 (Gibco). Following three washing steps in serum-free DMEM, the porogens were allowed to swell for 3 h, on a rocker at 4 °C. The swollen porogens were centrifuged at 500 rcf and the excess fluid was removed.

Bone marrow-derived MSCs were isolated from two 3 month-old Sprague-Dawley rat (Charles River) as previously described [9] and expanded until passage 5. Cells pooled from the two donors were used for all animals in the study. MSCs were encapsulated in the bulk gel with a concentration analogous to previous studies [7]: for *in vitro* studies, $2*10^6$ MSCs/mL bulk gel (or $1*10^6$ MSCs/mL void-forming hydrogel); for *in vivo* surgeries, $20*10^6$ MSCs/mL void-forming hydrogel. For comparative purposes, only rat MSCs were used in both immunocompetent and T-cell deficient athymic RNU nude rats, although the latter is

Figures legends

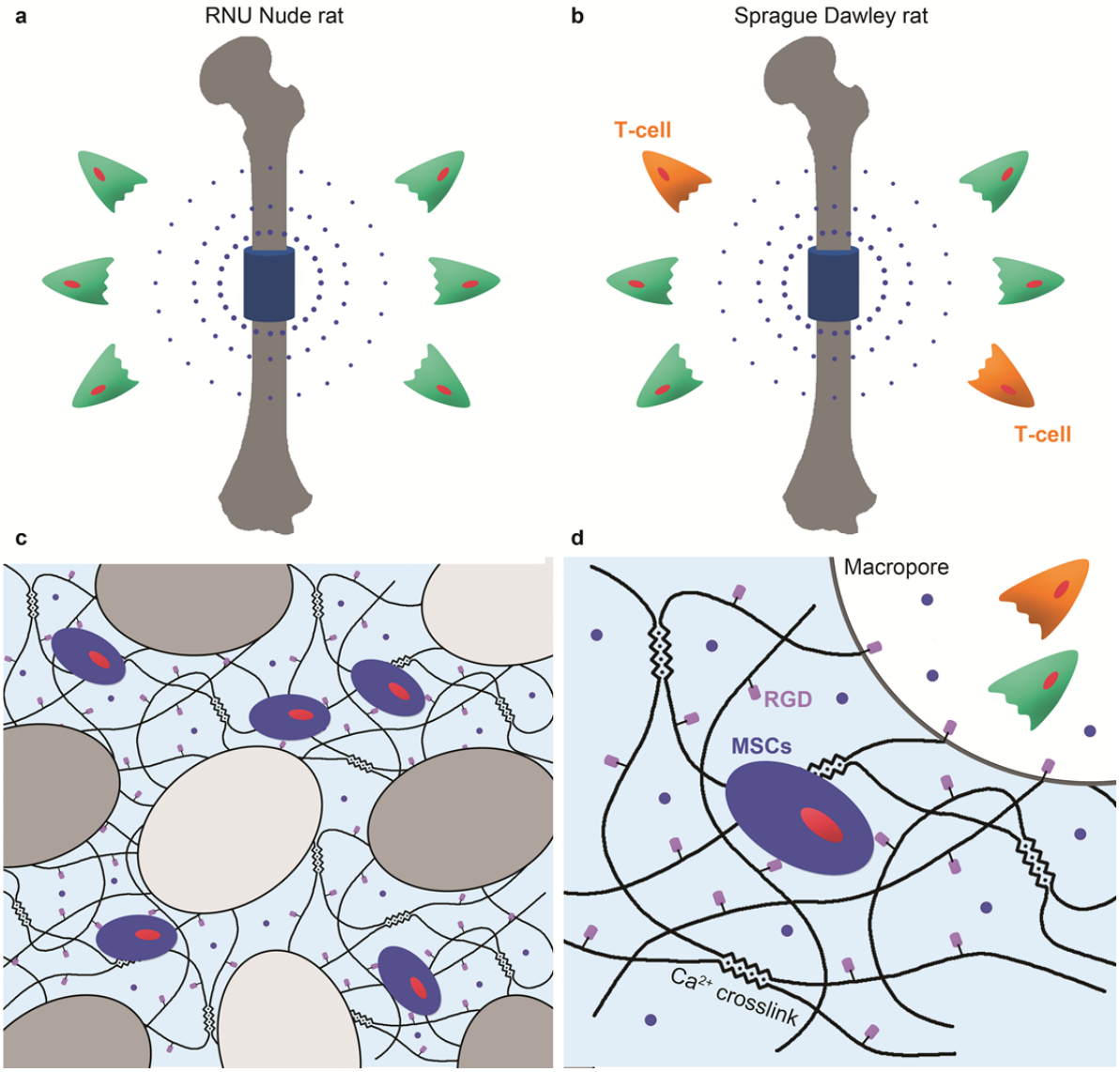

Figure 1. MSC-laden void-forming alginate hydrogels in critical-sized femoral defects of animals with different immune status. Endogenous cell migration towards MSC-laden void-forming alginate hydrogels in (a) T-cell deficient athymic RNU nude rats and (b) immunocompetent Sprague Dawley rats. (c) RGD-modified (violet), ionically crosslinked (Ca^{2+} crosslink) alginate hydrogels with encapsulated MSCs (blue) in the bulk phase and fast-degrading alginate porogens (grey to white) to impart a macroporous architecture. (d) Encapsulated MSCs (blue) sense the bulk hydrogel stiffness optimized to foster osteogenic differentiation, while the emerging macroporous architecture facilitates paracrine signaling (blue molecules), endogenous cell (green/orange) migration, proliferation and tissue formation.

commonly used to evaluate the regeneration potential of biomaterials in combination with cells of human origin.

The MSC-laden, 2% w/v bulk hydrogel, optimized for osteogenic differentiation [7], was mixed with the swollen porogens in a 1:1 ratio, using two syringes and a luer-lock connector (Bio-Rad Laboratories). The mixture of the bulk hydrogel, MSCs and porogens was ionically crosslinked with 4% v/v $CaSO_4$ (1.22 M), poured into molds and cast for 30 min. The molds had the following dimensions: 8 mm diameter, 3 mm height, for *in vitro* characterization, and 4 mm diameter, 5.5 mm height, for *in vivo* implantation. After casting, hydrogels for *in vitro* studies were transferred to 24-well plates, with DMEM supplemented with 10% fetal calf serum (FCS Superior, Biochrom), 1% penicillin/streptomycin (P/S) (Biochrom) and 1% glutamax (Life Technologies), and incubated at 37 °C and 5% CO_2. Hydrogels for surgeries were transferred to serum-free DMEM and stored at 4 °C until implantation, to slow down cell metabolism and prevent nutrient shortage. This ensured that all four animals operated within 1-3 h (in one day) received gels containing cells with a similar metabolic activity.

Biomechanical testing

The initial stiffness of the hydrogels was measured on equilibrated hydrogels after incubation for 2 h in DMEM, with 1% P/S, at 37 °C and 5% CO_2. The elastic modulus (E) was determined by unconfined compression testing (BOSE ElectroForce), in air at room temperature. The hydrogels were not hydrated during the 90 s duration of the test. A load cell of 1000 g and a deformation rate of 0.025 mm/s were applied. The elastic modulus was calculated based on the slope of the stress-strain curve in the initial 0-10% linear elastic deformation range. The diameter of the gels was determined using calipers. A total of n = 6 bulk gels and n = 3 void-forming gels were measured.

Degradation properties

Following biomechanical testing, the mass of the swollen gels (M_{wet}) was measured at 2 h, day 1, 3 and 7. Next, the gels were quick-frozen in liquid nitrogen and stored at -80 °C. After lyophilization, the dry mass (M_{dry}) and mass swelling ratio $(M_{wet}-M_{dry})/M_{dry}$ were determined for n = 6 bulk gels and n = 3 void-forming hydrogels.

Microstructural analysis

The architecture of the macroporous hydrogel was investigated using a scanning electron microscope (SEM) (FEI FEG-ESEM Quanta 600). After quick-freezing and lyophilization, each gel was immersed in liquid nitrogen and halved using two forceps. The generated fracture surface was sputtered with gold and platinum to make the sample conductive. SEM images were taken using high vacuum, at an accelerating voltage of 4-5 kV, a working distance of 6.2-7.4 mm and a spot size of 4.0.

Viability of encapsulated MSCs in vitro

The viability of encapsulated MSCs in bulk gels and in void-forming hydrogels was investigated using a LIVE/DEAD viability/cytotoxicity kit (Invitrogen). Cell-laden hydrogels were incubated in DMEM, with 10% FCS, 1% P/S, 1% glutamax, at 37 °C and 5% CO_2, for 1 h and 7 days. Images were obtained using a confocal/multi-photon laser scanning microscope (Leica TCS SP5 and MaiTai laser system, Spectra Physics, Germany) and a 25 x 0.95 water immersion objective. An area of 620 x 620 μm^2 was imaged in a 300 µm z-stack with 4 µm step size.

Animal model and surgical approach

All animal experiments were carried out according to the NIH Guide for Care and Use of Laboratory Animals. The study was approved by the local legal representative (LaGeSo Berlin, G0167/11). T-cell deficient athymic RNU nude female rats (Crl:NIH-*Foxn1*^{rnu}) and immunocompetent Sprague Dawley female rats were used for the study (Charles River). At the date of surgery, athymic RNU nude rats were 10 weeks-old (138-167 g) and Sprague Dawley rats, 20 weeks-old (310-390 g). The group immunocompetent Sprague Dawley rats with an empty hydrogel was published elsewhere [9] and is included for comparison purposes. At the date of surgery, these animals were 12 weeks-old (260-280 g).
The surgical approach has been previously reported.[9, 23, 24] In short, for general anesthesia Sprague Dawley rats received an intraperitoneal injection of medetomidine (0.3 mg/kg, Domitor, Pfizer) and ketamine (60 mg/kg, Ketamin, Actavis). For the smaller and lighter athymic RNU nude rats, anesthesia was administered via isoflurane through a custom-made mask (2% in 0.8-1.5 l of O_2/min). The eyes were protected from dehydration by

covering with ointment (Bepanthen, Jenapharm). A 5 mm critical-sized segmental defect was created in the diaphysis of the left femur. After stabilizing the femur, a double transverse osteotomy was created with an oscillating saw. The hydrogels with 4 mm diameter and 5.5 mm height (**Figure 2**a) were placed into the defect under pre-compression (Figure 2b). For Sprague Dawley rats, a custom-made, rigid, external fixator was used [9], while for athymic RNU nude rats an ExFixRat fixator (RISystem) was employed due to their smaller size (Figure 2b-c). Both fixation systems are classified as rigid fixators that can withstand the weight bearing of the animal after creating a 5 mm segmental defect.[25, 26] For post-operative analgesia, rats received a subcutaneous injection of tramadol hydrochloride (20 mg/kg, Tramal, Gruenenthal). As preventive antibiotic, a subcutaneous injection of clindamycine (45 mg/kg, Ratiopharm GmbH) was administered. The animals were sacrificed 6 weeks post-surgery. The femora were dissected and fixed in 4% paraformaldehyde (PFA) (Carl-Roth GmbH) for 24 h, at 4°C. The samples were dehydrated by incubating in ascending sucrose solutions (10%, 20% and 30% sugar dissolved in distilled water), each step for 24 h at 4°C. Afterwards the samples were stored in PBS at 4°C.

High-resolution ex vivo microcomputed tomography

High-resolution *ex vivo* microcomputed tomography (microCT) (VivaCT 40, Scanco Medical AG) scans were performed for both animal groups at 6 weeks post-surgery. Prior to the measurements, the fixator was disassembled and the pins removed. The scans were performed at 70 kilovolt peak (kVp), 114 µA current, 10.5 µm voxel size and 381 ms exposure (integration) time. A 0.5 mm aluminum filter was used to remove low-energy photons and reduce artifacts caused by beam hardening.

The volume of interest (VOI) analyzed included the 5 mm segmental defect and additional 0.5 mm from the proximal and distal osteotomies. A low pass Gaussian filter of a width 0.8 pixels and support of 1.0 was used to remove the noise. A semi-automated segmentation of cross-sectional tomograms was performed. The periosteal and endosteal callus were defined by an outer and inner boundary, respectively and the cortical bone was excluded.

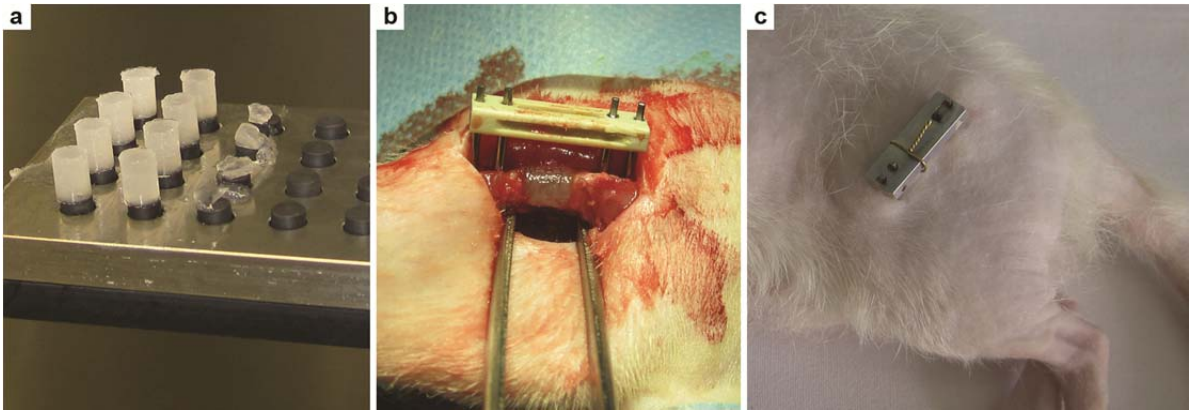

Figure 2. Hydrogel implantation in a 5 mm critical-sized rat femoral defect. (a) Cylindrical void-forming alginate hydrogels loaded with $20*10^6$ MSC/mL are implanted in a 5 mm critical-sized femoral defect in immunocompetent Sprague Dawley rats and (b, c) T-cell deficient athymic RNU nude rats, previously stabilized with a rigid external ExFixRatTM fixation system (RISystem AG), (b) during and (c) after surgery.

A global threshold of 482.7 mg HA/cm³ (2316 HU) was determined based on the grey scale histograms of the segmented VOI for each sample and averaging for all groups.[27]

Within the VOI, the following parameters were analyzed: ratio of bone volume to total callus volume (BV/TV, %), bone mineral density (BMD, mg hydroxyapatite/cm^3) and tissue mineral density (TMD, mg hydroxyapatite/cm^3). BMD and TMD were obtained comparing the X-ray attenuation using hydroxyapatite standards with the attenuation in the specimen. BMD comprises mineralized and non-mineralized voxels in the total callus volume, while TMD only contains mineralized voxels.[27]

Histology and histomorphometry

Freeze embedding of the femora was performed following the method of the SECTION-LAB Co. Ltd. (Hiroshima, Japan). A metal mold was placed in cooled n-hexane and filled with embedding medium (SCEM, SECTION-LAB Co. Ltd.). The femora were placed inside the mold with the former fixator side facing upwards. Cryosections with a thickness of 7 μm were cut following the Kawamoto method [28] using a Leica CM1950 cryotome (Leica Microsystems). To cut cryosections of undecalcified bone, a thin adhesive plastic film (C9 cryofilm, SECTION-LAB Co. Ltd.) was pressed to the cutting surface before sectioning. The section was then attached to a microscopic slide, air-dried for 45 min and stored at -80 °C.

Sections were stained with Movat Pentachrome to visualize collagen and mineralized tissue (yellow), cartilage (blue-green), connective tissue (light blue), muscle (red), cell nuclei (black) and cell cytoplasm (light red).[29] Images were acquired with an Axioscope 2.0 (Zeiss) and AxioVision software (Zeiss) in 2.5x magnification. Quantitative histomorphometry was performed using the software ImageJ.[30] First, the endosteal fracture gap area and total defect area were determined using the proximal and distal cortical bone ends as landmarks. Thresholding according to their respective color was used to segment bone, cartilage, prolapsed muscle and connective tissue areas and percentages of the endosteal fracture gap were calculated. The remaining alginate hydrogel area in the total defect area was calculated in mm^2 and expressed as a percentage of the initial longitudinal cross-sectional alginate area (20 mm^2). The results for empty gels were

published elsewhere [9] and were included for comparison purposes, after having been re-evaluated by the same person analyzing the new groups, for consistency.

Endogenous cell migration into the defect was measured for each animal based on five images within the defect region, in 40x magnification. The cells were classified based on morphology, as described previously [9]. Briefly, lymphocyte-like morphology included cells with circular shape and large nucleus, while non-lymphocyte morphology included cells with a small nucleus and variable shape. Cells without a visible nucleus were not included in the analysis. For each image, the number of cells per mm^2 was calculated manually. The mean value of five images per animal was obtained. Finally the median of each group was plotted in a box plot.

Statistical analysis

The groups under investigation were: (i) immunocompetent Sprague Dawley rats with MSC-laden gels (n = 4 out of 8 operated for both microCT and histology) and (ii) T-cell deficient athymic RNU nude rats with MSC-laden gels (n = 6/8 for microCT, 5/8 for histology). The group immunocompetent Sprague Dawley rats with an empty hydrogel was published elsewhere [9] and was included for comparison purposes, after having been re-evaluated by the same person analyzing the new groups, for consistency (n = 4/9 for *ex vivo* microCT, 6/9 for histology). A larger number of animals per group were operated but not included in the analysis. Exclusion criteria were pin loosening, osteolysis, humane early sacrifice or gel dislocation out of the defect site.

The data is presented in form of box plots showing the median, first and third quartiles, and minimum and maximum values indicated by error bars. Outliers are marked with stars. The statistical analysis was carried out with the non-parametric, two-tailed Mann-Whitney U test (SPSS 18.0). A confidence level of 95% was used (p = 0.05). For multiple pair-wise comparisons, the p-values were adjusted according to Bonferroni-Holm post-hoc analysis. Statistically significant differences are indicated with an asterisk on a horizontal line pointing at the pair-wise comparison.

Results

In vitro characterization of MSC-laden alginate hydrogels

Bulk alginate hydrogels with a stiffness optimized for osteogenic differentiation were synthesized.[5, 7] Unconfined compression testing at day 0 confirmed an initial target bulk hydrogel stiffness of 66.6 ± 7.8 kPa (n = 6), which dropped to 40.3 ± 3.0 kPa at day 3 due to diffusion of crosslinking calcium ions and then exhibited a plateau (**Figure 3**a). Void-forming gels with a 1:1 ratio of fast-degrading alginate porogens to bulk polymer exhibited an initial stiffness of 37.7 ± 2.5 kPa (n = 3), which dropped to 3.5 ± 0.5 kPa at day 3 (Figure 3a). The hydrolytically degradable alginate porogens are shown in a SEM micrograph of a flash-frozen fractured surface of a void-forming hydrogel (Figure 3b). The changes in dry weight and mass swelling ratio with time confirmed the porogen degradation in void-forming hydrogels, while the bulk gels remained stable over time (Figure 3c, d).

Bulk hydrogels foster high viability of encapsulated cells, which exhibited a round morphology after 7 days (**Figure 4**a, b), while MSCs in void-forming gels had spread morphology (Figure 4c, d). Despite the higher cell density in gels for *in vivo* surgeries, the viability prior to implantation was high (Figure 4e) and cell-free areas corresponding to the fast degrading porogens were visible (Figure 4e, f).

High-resolution ex vivo microCT of mineralized tissue

Bone regeneration in 5 mm critical-sized femoral defects, filled with void-forming hydrogel only and gel + MSCs groups, was evaluated 6 weeks post-surgery using high-resolution *ex vivo* microcomputed tomography (microCT) (**Figure 5**). A higher value of bone volume fraction was observed for the athymic RNU nude rats with MSC-laden gels compared with immunocompetent Sprague Dawley rats, although the difference was not statistically significant ($p = 0.114$) (Figure 5a). Similarly, bone mineral density and tissue mineral density, which are indicators of the quality of newly formed bone, were higher for athymic RNU nude rats, albeit the differences were not statistically significant ($p = 0.114$ and $p = 0.171$, respectively) (Figure 5b, c). 3D renderings of *ex vivo* microCT scans of one representative sample per group are shown in Figure 5d-f.

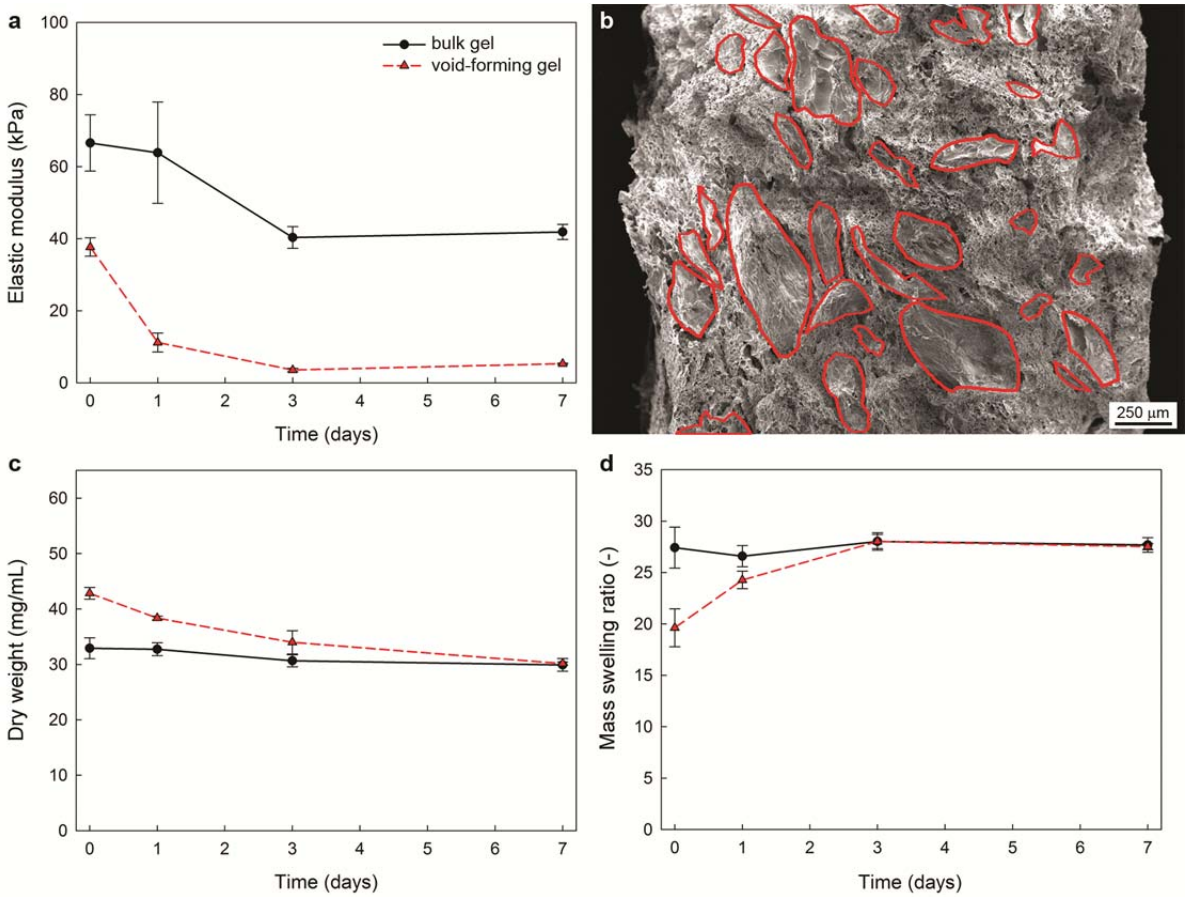

Figure 3. *In vitro* characterization of alginate hydrogels. (a) Unconfined compression testing of bulk (n = 6) and void-forming composite (n = 3) hydrogels. (b) SEM micrograph of flash-frozen fractured surface of a void-forming hydrogel showing the fast-degrading alginate porogens (marked in red). (c) Dry weight and (d) mass swelling ratio of bulk (n = 6) and void-forming (n = 3) hydrogels.

In vivo endogenous cell migration

Besides the ability to differentiate into different lineages, MSCs can also support tissue regeneration through the secretion of bioactive molecules and recruitment of endogenous cells. To investigate the endogenous cell migration *in vivo* at week 6, the cell number at the defect site of the void-forming hydrogel only and gel + MSCs groups were compared (**Figure 6**a). The total number of cells, cells with lymphocyte-like morphology and cells with non-lymphocyte morphology were quantified on histological images. A higher total number of cells was observed in the defect area with MSC-laden gels compared to the hydrogel only group. This difference was significant for athymic RNU nude rats ($p = 0.017$), with a higher fraction of cells with non-lymphocyte morphology ($p = 0.04$). The number of cells with lymphocyte-like morphology was lowest for the athymic RNU nude rats, as expected. Representative histological images of the gels with MSCs in immunocompetent Sprague Dawley rats (Figure 6b, c) and athymic RNU nude rats (Figure 6d, e) show that most of the cells in the defect site reside in the tissue surrounding alginate fragments (Alg), and a smaller fraction of cells are encapsulated in the hydrogel.

In vivo tissue formation and hydrogel degradation

Newly formed bone, cartilage, prolapsed muscle and connective tissue (in % of the endosteal fracture gap) were analyzed by histology and histomorphometry 6 weeks post-surgery (**Figure 7**a). Alginate hydrogels prevented muscle prolapse but no statistically significant differences in bone, cartilage or connective tissue formation were found between the groups. The endosteal fracture gap of immunocompetent Sprague Dawley rats (Figure 7b) and athymic RNU nude rats (Figure 7c) was mainly filled with connective tissue and islands of remaining alginate hydrogel (dark green). The latter was quantified as % of the initial hydrogel area (Figure 7a) and was visible in the form of small hydrogel fragments (Alg) and empty circular spaces surrounded by a fibrous capsule (FibC) (Figure 7d-f). The empty space is believed to be a sample preparation artefact and indicates that the alginate was less infiltrated with connective tissue and less degraded. A thick fibrous capsule was found in athymic RNU nude rats (Figure 7d-e), while a thinner fibrous capsule was observed in immunocompetent Sprague Dawley rats (Figure 7f). Ossification islands

(yellow) were observed originating from alginate fragments in both animal groups (Figure 7g-i).

Discussion

Biomaterials with tunable biophysical properties captured the interest of the tissue engineering community.[5, 7] The adaptive immune system and lymphocytes, in particular, play a role in bone regeneration.[16-18] In this study, we compare the regenerative potential of MSC-laden, void-forming alginate hydrogels, with a bulk stiffness optimized for osteogenic differentiation, using a critical-sized segmental femoral defect model in two different animal models: T-cell deficient athymic RNU nude rats and immunocompetent Sprague Dawley rats.

Void-forming alginate hydrogels were fabricated with an ionically crosslinked alginate bulk phase and degradable alginate porogens, as confirmed by the drop in overall elastic modulus from 37.7 ± 2.5 kPa to 5.3 ± 0.2 kPa over 7 days, decrease in dry weight (in units of mg/mL to normalize for gels of different size) and increase in mass swelling ratio (Figure 3). The initial bulk stiffness of 66.6 ± 7.8 kPa, dropped to 40.3 ± 3.0 due to calcium ion exchange after 3 days and remained stable thereafter (Figure 3a). These values are within the range previously reported to induce osteogenic differentiation.[5, 7] Cell viability was high after 7 days, spread cell morphology was observed in void-forming hydrogels, while cells remained round in the absence of porogens (Figure 4).

MicroCT analyses 6 weeks post-surgery revealed that the bone volume fraction, bone mineral density and tissue mineral density were higher for athymic RNU nude rats with MSC-laden gels compared with immunocompetent Sprague Dawley rats, although the differences were not statistically significant (Figure 5). However, this cell-laden void-forming alginate hydrogel was insufficient to fully bridge a critical-sized segmental femoral defect in either athymic RNU nude rats or immunocompetent Sprague Dawley rats. This is consistent with the previous study by Huebsch and colleagues, where less than 15% of the critical-sized cranial defect in athymic RNU nude rats was filled after 3 months, in the case of alginate hydrogels with optimized bulk stiffness.[7] Similarly, in the study by Darnell and colleagues, less than 20% of the critical-sized cranial defect in athymic RNU nude rats was

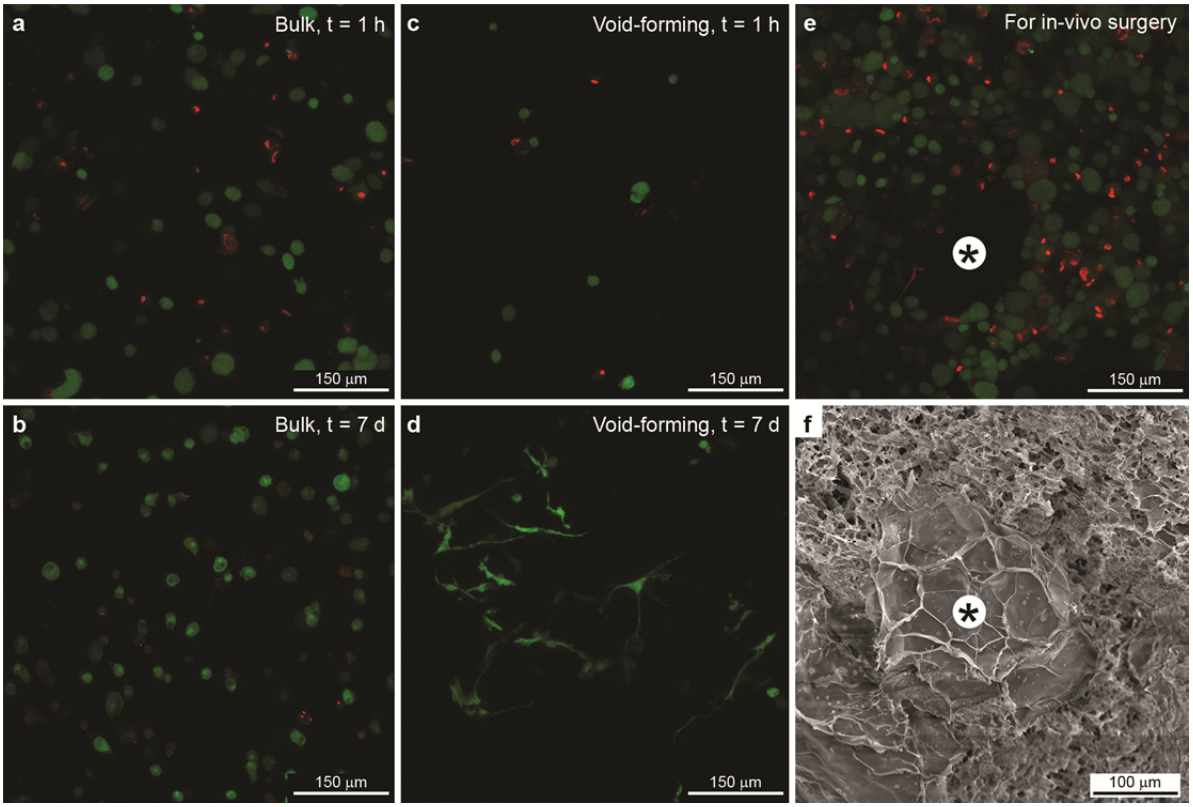

Figure 4. Viability of encapsulated MSCs *in vitro*. $2*10^6$ MSCs/mL bulk gel after (a) 1 hour and (b) 7 days. $1*10^6$ MSCs/mL void-forming gel ($2*10^6$ MSCs/mL bulk gel) after (c) 1 hour and (d) 7 days. (e) $20*10^6$ MSCs/mL void-forming gel prior to *in vivo* implantation, showing cell-free areas (*) corresponding to fast-degrading porogens. (f) SEM micrograph of flash-frozen fractured surface of a void-forming hydrogel showing a fast-degrading porogen. Live-dead staining (green: viable cell, red: dead cell), imaging depth 300 µm.

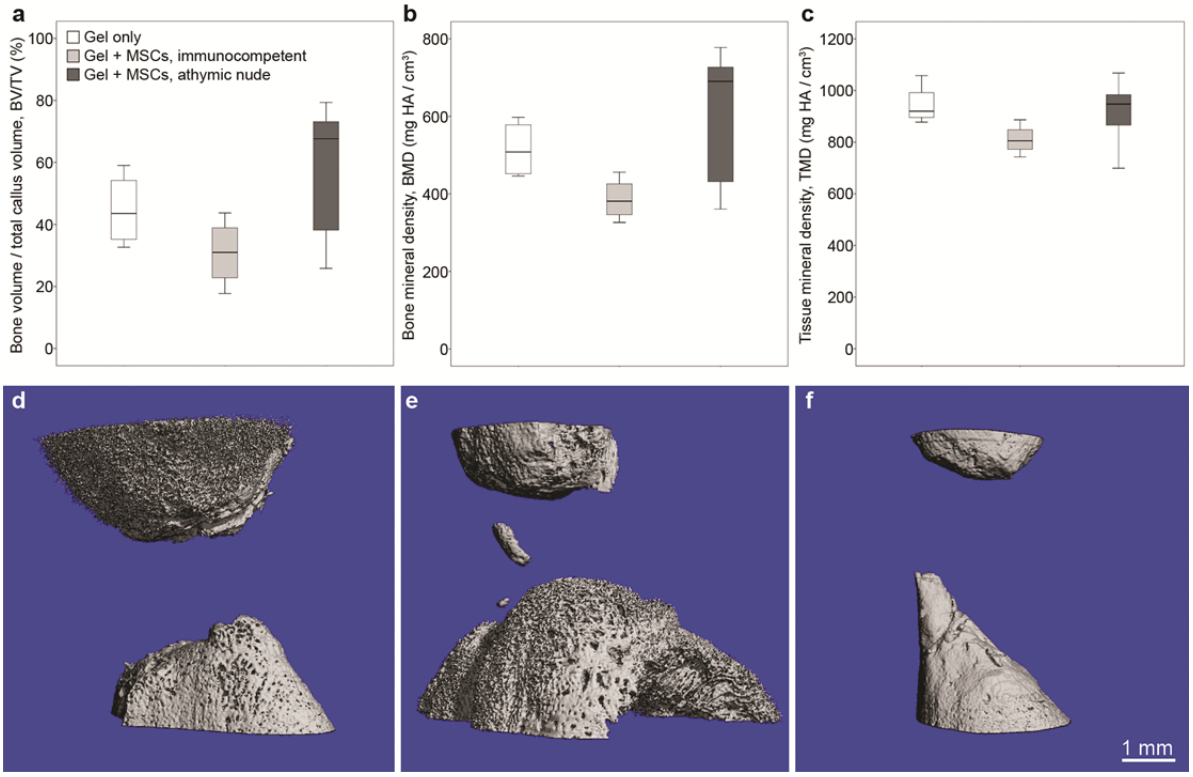

Figure 5. High-resolution e*x vivo* microCT of mineralized tissue after 6 weeks. (a) Bone volume fraction (BV/TV), (b) bone mineral density (BMD) and (c) tissue mineral density (TMD) of defects filled with gels indicated in (a). MicroCT 3D renderings of representative defects treated with (d) empty gels in immunocompetent Sprague Dawley rats with a bulk stiffness optimized for osteogenic differentiation (n = 4 out of 9 operated), gels with MSCs in (e) immunocompetent Sprague Dawley rats (n = 4/8) and (f) T-cell deficient athymic RNU nude rats (n = 6/8). A larger number of animals per group were operated but not included in the analysis. Exclusion criteria were pin loosening, osteolysis, humane early sacrifice or gel dislocation out of the defect site. Statistics: Two-tailed Mann-Whitney U test, $p < 0.05$, post-hoc Bonferroni-Holm. The results for empty gels were published elsewhere [9] and were re-evaluated and included for comparison purposes.

filled after 3 months, when implanting fast relaxing alginate hydrogels.[8] In the case of a load-bearing segmental femoral defect, such insufficient bone regeneration can lead to complications such as fixation loosening and osteolysis. This explains the lower number of analyzed vs. operated animals in this study.

Quantification of cell number at the defect site showed higher total number of cells in the defect area with MSC-laden gels compared to the hydrogel only group, with a significantly higher number of total cells and cells with non-lymphocyte morphology for athymic RNU nude rats (Figure 6). Encapsulated cells in alginate fragments were still visible after 6 weeks, although most of the cells were spread in the surrounding connective tissue (Figure 6b-e). This increased cell number could be attributed to (i) cells migrating outward from the bulk alginate and (ii) endogenous cell migration triggered by MSC paracrine signaling, as reported in previous studies.[11-15] Cell recruitment via MSC paracrine signaling seems to be more potent than the previously described SDF-1α induced effect, where a lower number of total cells and a higher number of immune cells with lymphocyte-like morphology were observed.[9] Qazi and colleagues reported a stronger paracrine effect when MSCs were seeded in microporous alginate cryogels vs. encapsulated in nanoporous hydrogels, due to enhanced diffusion of molecules and cell-cell contact.[14] This finding would speak for a strong MSC paracrine signaling in void-forming alginate hydrogels, where macropores emerge as the porogens degrade.

With regard to hydrogel degradation, the lower number of cells with lymphocyte-like morphology in the athymic RNU nude rats (Figure 6a) is consistent with the higher fraction of remaining alginate in the defect area (Figure 7a), compared to immunocompetent Sprague Dawley, which exhibit a lower fraction of remaining alginate. Interestingly, the remaining alginate fragments in the defect area of athymic RNU nude rats are surrounded by a thicker fibrous capsule (Figure 7d-e) compared to immunocompetent Sprague Dawley rats (Figure 7f). It is widely accepted that the innate immune system, and macrophages in particular, orchestrate the foreign body reaction and the inability to resolve chronic inflammation triggers fibroblast recruitment and formation of a fibrotic capsule.[31] However, recent research is now elucidating the role of the adaptive immune system, in particular that of T-cells, in directing innate immune response to implanted biomaterials,

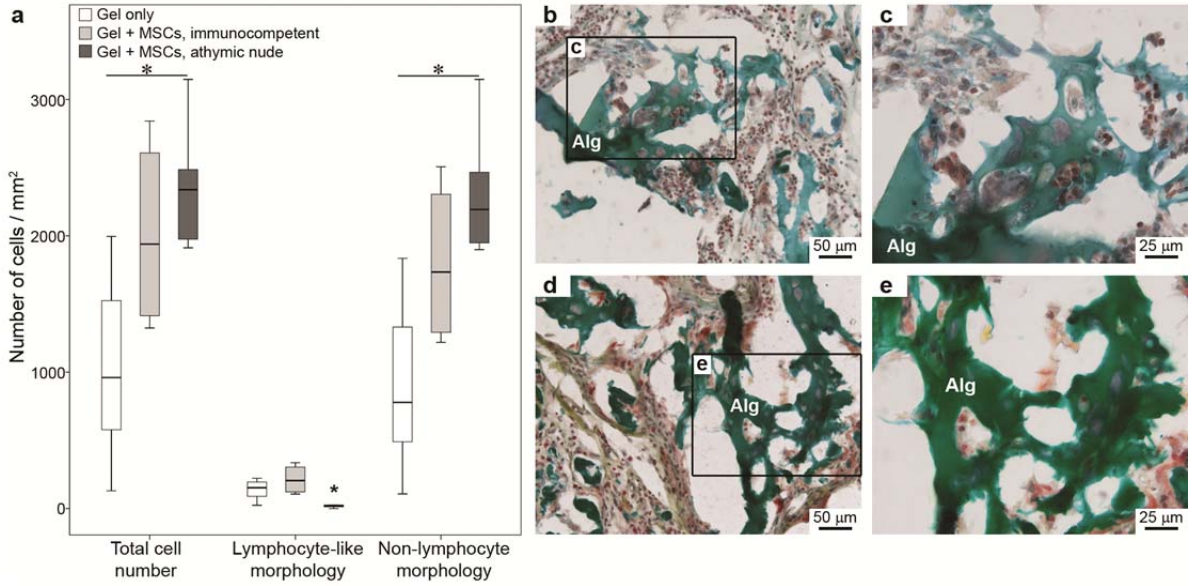

Figure 6. *In vivo* endogenous cell migration through paracrine effect of *ex vivo* encapsulated MSCs. (a) Quantification of the number of cells migrating into the defect site after 6 weeks. Representative histological images of the gels with MSCs in (b, c) immunocompetent Sprague Dawley rats (n = 4/8) and (d, e) athymic RNU nude rats (n = 5/8), with visible alginate hydrogel fragments (Alg), endogenous cell migration and (c, e) implanted MSCs encapsulated in the gel. Movat Pentachrome staining. Statistics: Two-tailed Mann-Whitney U test, $p < 0.05$, post-hoc Bonferroni-Holm. The results for empty gels in immunocompetent Sprague Dawley rats were published elsewhere [9] and were included for comparison purposes.

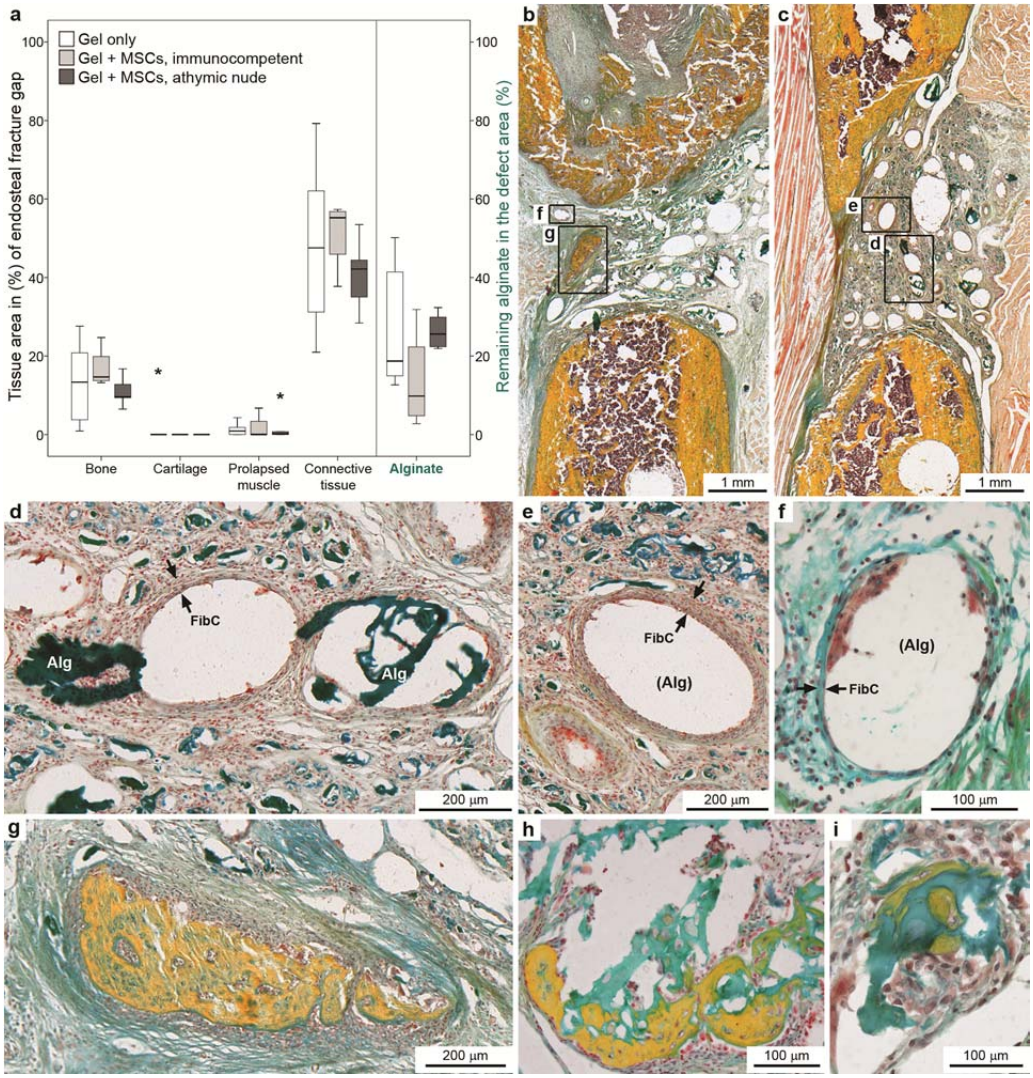

Figure 7. *In vivo* tissue formation, hydrogel degradation and ossification islands. (a) Newly formed bone, cartilage, prolapsed muscle and connective tissue in % of the endosteal fracture gap, stained with Movat Pentachrome and analyzed by histomorphometry 6 weeks post-surgery. Representative histological images of the gels with MSCs in (b) immunocompetent Sprague Dawley rats (n = 4/8) and (c) athymic RNU nude rats (n = 5/8). (d-f) Detail of large alginate fragments (Alg) surrounded by fibrous capsules (FibC, thickness indicated by two arrows) and smaller islands of alginate residues. (g-i) Ossification islands (yellow) originating from alginate fragments suggest that encapsulated cells did differentiate in the osteogenic lineage and started to mineralize alginate. Statistics: Two-tailed Mann-Whitney U test, $p < 0.05$, post-hoc Bonferroni-Holm. The results for empty gels in immunocompetent Sprague Dawley rats were published elsewhere [9] and were re-evaluated and included for comparison purposes.

resolution of inflammation and tissue repair.[32] Thus, the altered balance between innate and adaptive immune response should be taken into consideration when T-cell deficient athymic RNU nude rats are used in studies investigating tissue regeneration.

The ossification islands originating from alginate fragments suggest that encapsulated cells differentiated into the osteogenic lineage and started to mineralize the alginate hydrogel (Figure 7g-i). However, this effect was not sufficient to bridge the critical-sized segmental femoral defect with mineralized tissue.

Conclusions

The regenerative potential of MSC-laden, void-forming alginate hydrogels was evaluated in load-bearing, 5 mm critical-sized segmental femoral defects, in both T-cell deficient athymic RNU nude rats and immunocompetent Sprague Dawley rats. Differences in mineralized tissue formation, endogenous cell migration and *in vivo* hydrogel degradation were observed between both animal models with different immunity. Bone volume fraction, bone mineral density and tissue mineral density were higher for athymic RNU nude rats, although the differences were not statistically significant. A significantly higher number of total cells and cells with non-lymphocyte morphology were found for athymic RNU nude rats, while the number of cells with lymphocyte-like morphology was lower, as expected. Hydrogel degradation was slower and the remaining alginate fragments were surrounded by a thicker fibrous capsule in athymic RNU nude rats compared to immunocompetent Sprague Dawley rats.

There seems to be a strong paracrine signaling from the MSCs encapsulated in the bulk alginate that attracts endogenous cells to the defect site, with a lower fraction of inflammatory cells compared to previously reported hydrogels containing SDF-1α.[9] Ossification islands originating from alginate residues suggest that encapsulated MSCs differentiated into the osteogenic lineage and initiated the mineralization process. However, this effect was insufficient to fully bridge the bone defect in both animal models. In conclusion, alginate hydrogels can be used to deliver MSCs and thereby recruit endogenous cells through paracrine signaling, but additional osteogenic stimuli, such as

growth factor delivery,[33-35] are needed to regenerate critical-sized segmental femoral defects.

Acknowledgements

This work was supported by the Rahel-Hirsch Fellowship (A.C.) and the Lydia-Rabinowitsch Stipendium (A.C.), both from the Commission for Women´s Advancement, Charité - Universitätsmedizin Berlin, the Deutsche Forschungsgemeinschaft DFG CI 203/1-2 (A.C.) and DFG FOR 2165 (K.S.), the Berlin-Brandenburg Center for Regenerative Therapies (BCRT) and the Einstein Foundation Berlin (D.J.M., G.N.D.). We thank E. Lippens and A. Lueckgen, at Charité - Universitätsmedizin Berlin, and N. Huebsch at Harvard University, for useful discussions. We would also like to thank M. Thiele, G. Korus, A. Kadow-Romacker and L. Schumann, at Charité - Universitätsmedizin Berlin, and S. Weichold at the Max Planck Institute of Colloids and Interfaces, for technical assistance.

Author Disclosure Statement

No competing financial interests exist.

Author contribution

A.C., G.N.D. and D.J.M. conceived the idea. A.C. wrote the manuscript. A.C., D.S.G., K.S., A.E. and A.D. carried out the experiments and evaluated the data. K.S. and A.E. performed the surgeries. L.G. provided the raw materials for the synthesis of void-forming hydrogels. All authors contributed to the interpretation of the results and commented on the manuscript.

References

1. Roddy, E., DeBaun, M.R., Daoud-Gray, A., Yang, Y.P., and Gardner, M.J. Treatment of critical-sized bone defects: clinical and tissue engineering perspectives. Eur J Orthop Surg Traumatol **28**, 351, 2018.

2. Cipitria, A., and Salmeron-Sanchez, M. Mechanotransduction and Growth Factor Signalling to Engineer Cellular Microenvironments. Adv Healthc Mater **6**, 1700052, 2017.

3. Pelham, R.J., and Wang, Y.-L. Cell locomotion and focal adhesions are regulated by substrate flexibility. PNAS **94**, 13661, 1997.

4. Engler, A.J., Sen, S., Sweeney, H.L., and Discher, D.E. Matrix elasticity directs stem cell lineage specification. Cell **126**, 677, 2006.

5. Huebsch, N., Arany, P.R., Mao, A.S., Shvartsman, D., Ali, O.A., Bencherif, S.A., et al. Harnessing traction-mediated manipulation of the cell/matrix interface to control stem-cell fate. Nat Mater **9**, 518, 2010.

6. Chaudhuri, O., Gu, L., Klumpers, D., Darnell, M., Bencherif, S.A., Weaver, J.C., et al. Hydrogels with tunable stress relaxation regulate stem cell fate and activity. Nat Mater **15**, 326, 2016.

7. Huebsch, N., Lippens, E., Lee, K., Mehta, M., Koshy, S.T., Darnell, M.C., et al. Matrix elasticity of void-forming hydrogels controls transplanted-stem-cell-mediated bone formation. Nat Mater **14**, 1269, 2015.

8. Darnell, M., Young, S., Gu, L., Shah, N., Lippens, E., Weaver, J., et al. Substrate stress-relaxation regulates scaffold remodeling and bone formation in vivo. Adv Healthc Mater **6**, 1601185, 2017.

9. Cipitria, A., Boettcher, K., Schoenhals, S., Garske, D.S., Schmidt-Bleek, K., Ellinghaus, A., et al. In-situ tissue regeneration through SDF-1alpha driven cell recruitment and stiffness-mediated bone regeneration in a critical-sized segmental femoral defect. Acta Biomater **60**, 50, 2017.

10. Haugh, M.G., Vaughan, T.J., Madl, C.M., Raftery, R.M., McNamara, L.M., O'Brien, F.J., et al. Investigating the interplay between substrate stiffness and ligand chemistry in directing mesenchymal stem cell differentiation within 3D macro-porous substrates. Biomaterials **171**, 23, 2018.

11. Caplan, A.I., and Correa, D. The MSC: An Injury Drugstore. Cell Stem Cell **9**, 11, 2011.

12. Baraniak, P.R., and McDevitt, T.C. Stem cell paracrine actions and tissue regeneration. Regen Med **5**, 121, 2010.

13. Seebach, E., Freischmidt, H., Holschbach, J., Fellenberg, J., and Richter, W. Mesenchymal stroma cells trigger early attraction of M1 macrophages and endothelial cells into fibrin hydrogels, stimulating long bone healing without long-term engraftment. Acta Biomater **10**, 4730, 2014.

14. Qazi, T.H., Mooney, D.J., Duda, G.N., and Geissler, S. Biomaterials that promote cell-cell interactions enhance the paracrine function of MSCs. Biomaterials **140**, 103, 2017.

15. Wobma, H.M., Liu, D., and Vunjak-Novakovic, G. Paracrine effects of mesenchymal stromal cells cultured in three-dimensional settings on tissue repair. ACS Biomater Sci Eng **4**, 1162, 2018.

16. Schmidt-Bleek, K., Schell, H., Schulz, N., Hoff, P., Perka, C., Buttgereit, F., et al. Inflammatory phase of bone healing initiates the regenerative healing cascade. Cell Tissue Res **347**, 567, 2011.

17. Mountziaris, P.M., Spicer, P.P., Kasper, F.K., and Mikos, A.G. Harnessing and modulating inflammation in strategies for bone regeneration. Tissue Eng Part B Rev **17**, 393, 2011.

18. Claes, L., Recknagel, S., and Ignatius, A. Fracture healing under healthy and inflammatory conditions. Nat Rev Rheumatol **8**, 133, 2012.

19. Colburn, N.T., Zaal, K.J., Wang, F., and Tuan, R.S. A role for gamma/delta T cells in a mouse model of fracture healing. Arthritis Rheum **60**, 1694, 2009.

20. Toben, D., Schroeder, I., El Khassawna, T., Mehta, M., Hoffmann, J.-E., Frisch, J.-T., et al. Fracture healing is accelerated in the absence of the adaptive immune system. J Bone Miner Res **26**, 113, 2011.

21. Reinke, S., Geissler, S., Taylor, W.R., Schmidt-Bleek, K., Juelke, K., Schwachmeyer, V., et al. Terminally differentiated CD8(+) T cells negatively affect bone regeneration in humans. Sci Transl Med **5**, 177ra36, 2013.

22. El Khassawna, T., Serra, A., Bucher, C.H., Petersen, A., Schlundt, C., Konnecke, I., et al. T Lymphocytes Influence the Mineralization Process of Bone. Front Immunol **8**, 562, 2017.

23. Mehta, M., Schell, H., Schwarz, C., Peters, A., Schmidt-Bleek, K., Ellinghaus, A., et al. A 5-mm femoral defect in female but not in male rats leads to a reproducible atrophic non-union. Arch Orthop Trauma Surg **131**, 121, 2011.

24. Schwarz, C., Wulsten, D., Ellinghaus, A., Lienau, J., Willie, B.M., and Duda, G.N. Mechanical load modulates the stimulatory effect of BMP2 in a rat nonunion model. Tissue Eng Part A **19**, 247, 2013.

25. Wulsten, D., Glatt, V., Ellinghaus, A., Schmidt-Bleek, K., Petersen, A., Schell, H., et al. Time kinetics of bone defect healing in response to BMP-2 and GDF-5 characterised by in vivo biomechanics. Eur Cells Mater **21**, 177, 2011.

26. Glatt, V., and Matthys, R. Adjustable stiffness, external fixator for the rat femur osteotomy and segmental bone defect models. J Vis Exp, e51558, 2014.

27. Bouxsein, M.L., Boyd, S.K., Christiansen, B.A., Guldberg, R.E., Jepsen, K.J., and Muller, R. Guidelines for assessment of bone microstructure in rodents using micro-computed tomography. J Bone Miner Res **25**, 1468, 2010.

28. Kawamoto, T. Use of a new adhesive film for the preparation of multi-purpose fresh-frozen sections from hard tissues, whole-animals, insects and plants. Arch Histol Cytol **66**, 123, 2003.

29. Movat, H.Z. Demonstration of all connective tissue elements in a single section; pentachrome stains. AMA Arch Pathol **60**, 289, 1955.

30. Schneider, C., Rasband, W., and Eliceiri, K. NIH Image to ImageJ: 25 years of image analysis. Nat Methods **9**, 671, 2012.

31. Grainger, D.W. All charged up about implanted biomaterials. Nat Biotechnol **31**, 507, 2013.

32. Chung, L., Maestas, D.R., Housseau, F., and Elisseeff, J.H. Key players in the immune response to biomaterial scaffolds for regenerative medicine. Adv Drug Deliv Rev **114**, 184, 2017.

33. Simmons, C.A., Alsberg, E., Hsiong, S., Kim, W.J., and Mooney, D.J. Dual growth factor delivery and controlled scaffold degradation enhance in vivo bone formation by transplanted bone marrow stromal cells. Bone **35**, 562, 2004.

34. Kolambkar, Y.M., Dupont, K.M., Boerckel, J.D., Huebsch, N., Mooney, D.J., Hutmacher, D.W., et al. An alginate-based hybrid system for growth factor delivery in the functional repair of large bone defects. Biomaterials **32**, 65, 2011.

35. Dosier, C.R., Uhrig, B.A., Willett, N.J., Krishnan, L., Li, M.-T.A., Stevens, H.Y., et al. Effect of cell origin and timing of delivery for stem cell-based bone tissue engineering using biologically functionalized hydrogels. Tissue Eng Part A **21**, 156, 2015.

Dr. Amaia Cipitria, Ph.D.

Max Planck Institute of Colloids and Interfaces

Department of Biomaterials

14476 Potsdam, Germany

Tel: +49 (0)331 567-9452

Email: amaia.cipitria@mpikg.mpg.de